Skin substitute-assisted repair shows reduced dermal fibrosis in acute human wounds validated simultaneously by histology and optical coherence tomography

Nicholas S. Greaves, MBChB[1,3,4]; Syed A. Iqbal, PhD[1]; Tom Hodgkinson, PhD[1]; Julie Morris, MSc[2]; Brian Benatar, FRCPath[5]; Teresa Alonso-Rasgado, PhD[4]; Mohamed Baguneid, MD[3]; Ardeshir Bayat, MBBS, PhD[1,4]

1. Plastic and Reconstructive Surgery Research, Institute of Inflammation and Repair, The University of Manchester,
2. Department of Medical Statistics, University Hospital of South Manchester NHS Foundation Trust, Wythenshawe Hospital,
3. Department of Vascular Surgery, University Hospital of South Manchester NHS Foundation Trust, Wythenshawe Hospital, Manchester,
4. Bioengineering Group, School of Materials, University of Manchester, and
5. Department of Histopathology, The Pennine Acute Hospitals NHS Trust, The Royal Oldham Hospital, Oldham, United Kingdom

Reprint requests:
Dr. Ardeshir Bayat, Plastic and Reconstructive Surgery Research, Manchester Institute of Biotechnology (MIB), 131 Princess Road, Manchester M1 7ND, United Kingdom.
Tel/Fax: +0044 161 306 5177;
Email: ardeshir.bayat@manchester.ac.uk

Manuscript received: March 17, 2015
Accepted in final form: April 21, 2015

DOI:10.1111/wrr.12308

Related presentations: This paper was shortlisted in the Young Investigator award section of the European Tissue Repair Society (ETRS) annual meeting in October 2014 (Edinburgh, UK) and given as an oral podium presentation.

ABSTRACT

Skin substitutes are heterogeneous biomaterials designed to accelerate wound healing through provision of replacement extracellular matrix. Despite growing evidence for their use in chronic wounds, the role of skin substitutes in acute wound management and their influence on fibrogenesis remains unclear. Skin substitute characteristics including biocompatibility, porosity, and elasticity strongly influence cellular behavior during wound healing. Thus, we hypothesize that structural and biomechanical variation between biomaterials may induce differential scar formation after cutaneous injury. The following human prospective cohort study was designed to investigate this premise. Four 5-mm full thickness punch biopsies were harvested from 50 volunteers. In all cases, site 1 healed by secondary intention, site 2 was treated with collagen-GAG scaffold (CG), and decellularised dermis (DCD) was applied to site 3 while tissue extracted from site 4 was replaced (autograft). Healing tissue was assessed weekly with optical coherence tomography (OCT), before being excised on days 7, 14, 21, or 28 depending on study group allocation for later histological and immunohistochemical evaluation. Extracted RNA was used in microarray analysis and polymerase chain reaction of highlighted genes. Autograft treatment resulted in minimal fibrosis confirmed immunohistochemically and with OCT through significantly lower collagen I levels ($p = 0.047$ and 0.03) and reduced mean grayscale values ($p = 0.038$ and 0.015), respectively. DCD developed intermediate scar formation with partial rete ridge reformation and reduced fasiculonodular fibrosis. It was uniquely associated with late up-regulation of matrix metalloproteinases 1 and 3, oncostatin M, and interleukin-10 ($p = 0.007$, 0.04, 0.019, 0.019). Regenerated dermis was significantly thicker in DCD and autografts 28 days post-injury compared with control and CG samples ($p = 0.003$ and <0.0001). In conclusion, variable fibrotic outcomes were observed in skin substitute-treated wounds with reduced scarring in autograft and DCD samples compared with controls. OCT enabled concurrent assessment of wound morphology and quantification of dermal fibrosis.

αSMA	Alpha smooth muscle actin	MGV	Mean grayscale volume
CG	Collagen-GAG scaffold	MMP	Matrix metalloproteinase
CTGF	Connective tissue growth factor	OCT	Optical coherence tomography
d	Day	OSM	Oncostatin M
DCD	Decellularized dermis	qRT-PCR	Real time polymerase chain reaction
dSS	Dermal skin substitutes	TGF-β	Transforming growth factor beta
ECM	Extracellular matrix	TNF	Tumor necrosis factor
IL	Interleukin	VEGF	Vascular endothelial growth factor
LOX	Lysyl oxidase		

Wound healing is the means by which cutaneous damage is repaired, producing tissue, that is, functionally and cosmetically similar to uninjured skin.[1] Complex but coordinated interplay between multiple cell types, bioactive molecules, and extracellular matrix (ECM) proteins gives rise to recognized haemostatic, inflammatory, proliferative, and remodeling phases.[2,3] In adults, the normal end point of cutaneous repair is development of fibrotic scar tissue, which occurs after nearly all dermal injuries.[4,5] In contrast, fetal wound repair is regenerative, characterized by the absence of fibrosis and restoration of normal skin architecture.[5,6] This undesirable discrepancy in wound healing responses has largely been attributed to inflammation through athymic, transgenic, and knock-out murine studies. However, inherent differences in cellularity, cutaneous architecture, and bioactive molecular content between adult and fetal tissues are also crucial.[7–10] Studies investigating mechanisms by which inflammatory profibrotic stimuli can be limited to shift the balance from scarring to regeneration have predominantly focused on growth factors and other soluble mediators. Examples include manipulation of transforming growth factor-β (TGFβ), angiotensin peptides, and tissue inhibitors of metalloproteinases.[11–14] Despite this, therapies proven to ameliorate the fibrotic response to injury remain elusive.[11] In contrast, relatively little attention has been given to the influence of ECM characteristics on tissue repair. Indeed, reduced scarring was observed in rabbit incisional wounds after increasing fibromodulin expression using an adenoviral vector while the addition of hyaluronic acid to healing organ cultured limb explants of gestational day (d) 18 fetal mice promoted scarless repair.[12,15] Tissue engineered dermal skin substitutes (dSS) represent another method by which to artificially alter ECM components. These biomaterials fundamentally provide replacement ECM in the form of porous three-dimensional dermal templates to stimulate wound healing.[16] They are a relatively new therapeutic option in chronic wound management with a growing evidence base in diabetic and venous ulcers.[17,18] dSS vary significantly in their constituent proteins, morphology, and biomechanical properties.[19] These differences are likely to affect multiple wound healing processes including fibroplasia as ECM characteristics including porosity, elasticity, and biocompatibility strongly influence cellular migration, proliferation, and differentiation during healing.[20,21] However, studies investigating the possible use of dSS as a method of scar reduction are limited.[22,23]

Consequently, the aims of this unique human study were threefold. First, to identify differences in dermal fibrosis between wounds healing by secondary intention and those treated using skin substitutes. Second, to establish and quantify differences in fibrotic outcomes between collagen-GAG scaffold (CG), allograft (decellularised dermis [DCD]), and autograft-treated wounds, and finally, evaluate optical coherence tomography (OCT) as a noninvasive alternative to histology and collagen-based immunohistochemistry in assessment of cutaneous scarring and skin substitute-assisted wound healing.

MATERIALS AND METHODS

This prospective cohort study was performed in accordance with the Helsinki Declaration of 1975, National Research Ethics Service (reference number 12/NW/0078) and local research and development department (reference number 2011BP001) approval. Fifty volunteers meeting study inclusion/exclusion criteria (Supporting Information, Table S1) gave informed written consent to participate before being electronically randomized into one of five groups, containing 10 subjects (Figure 1A). The study was conducted at University Hospital South Manchester, England, U.K. Recruitment occurred between April and June 2013 while final follow-up was in July 2013.

On d0, four biopsy sites per subject were allocated with two on the right arm (sites 1 and 2) and two on the left (sites 3 and 4). Sites were located 2 cm proximal and 2 cm distal to the midpoint of a line connecting axillary hair line with medial epicondyle and investigated with OCT (Michelson Diagnostics Vivosight Topical OCT probe, Orpington, UK).

Five-millimeter full thickness punch biopsies (defined as extending to subcutaneous fat) were uniformly taken from each allocated site. In all cases, site 1 healed by secondary intention (Control), site 2 was treated with Integra Matrix Wound Dressing (CG; Integra LifeSciences, Plainsboro, NJ), site 3 was treated with National Health Service Blood and Transplant Decellularised Dermis (DCD; NHSBT, Watford, UK), and tissue excised from site 4 was replaced into the defect (Autograft). Neither CG nor DCD had epidermal components and was not epithelialised at the time of implantation. Wounds were covered with Tegaderm (3M, Bracknell, UK) for seven days, and patients given wound care advice.

Subjects attended follow-up on days 7, 14, 21, 28, and 42, where wounds were assessed with OCT. Group 1 subjects underwent 6-mm excision biopsies of healing tissue from sites 1–4 on d7, group 2 on d14, group 3 on d21, and group 4 on d28. Group 5 subjects did not undergo excision biopsies. All biopsied tissue was bisected with half placed in formalin and the remainder in RNA later for subsequent investigations (Figure 1B).

Dermal thickness was defined as distance between base of epidermis and subcutaneous fat, measured using Nanozoomer version 2.2.8 (Hamamatsu Photonics UK Limited, Welwyn Garden City, UK). Mean grayscale value (MGV) was derived from OCT and measured using image J software from a standardized area of upper reticular dermis. MGV evaluates light-scattering properties of a tissue, derived from the ratio of refractive indices of scattering centers to interstitial fluid.[24]

Laboratory techniques

Histology and immunohistochemistry (n = 10 patients/group)

Formalin-fixed paraffin-embedded tissue sections were prepared on glass slides and stained with haematoxylin and eosin as well as immunohistochemical markers for collagen I, collagen III, (Abcam, Cambridge, UK) alpha-smooth muscle actin (aSMA; Dako, Ely, UK), and fibronectin (Leica Biosystems, Newcastle, UK; Supporting Information, Table S2). Tissue Studio version 3.5.1 (Definiens, Munich, Germany) was used for stain analysis.

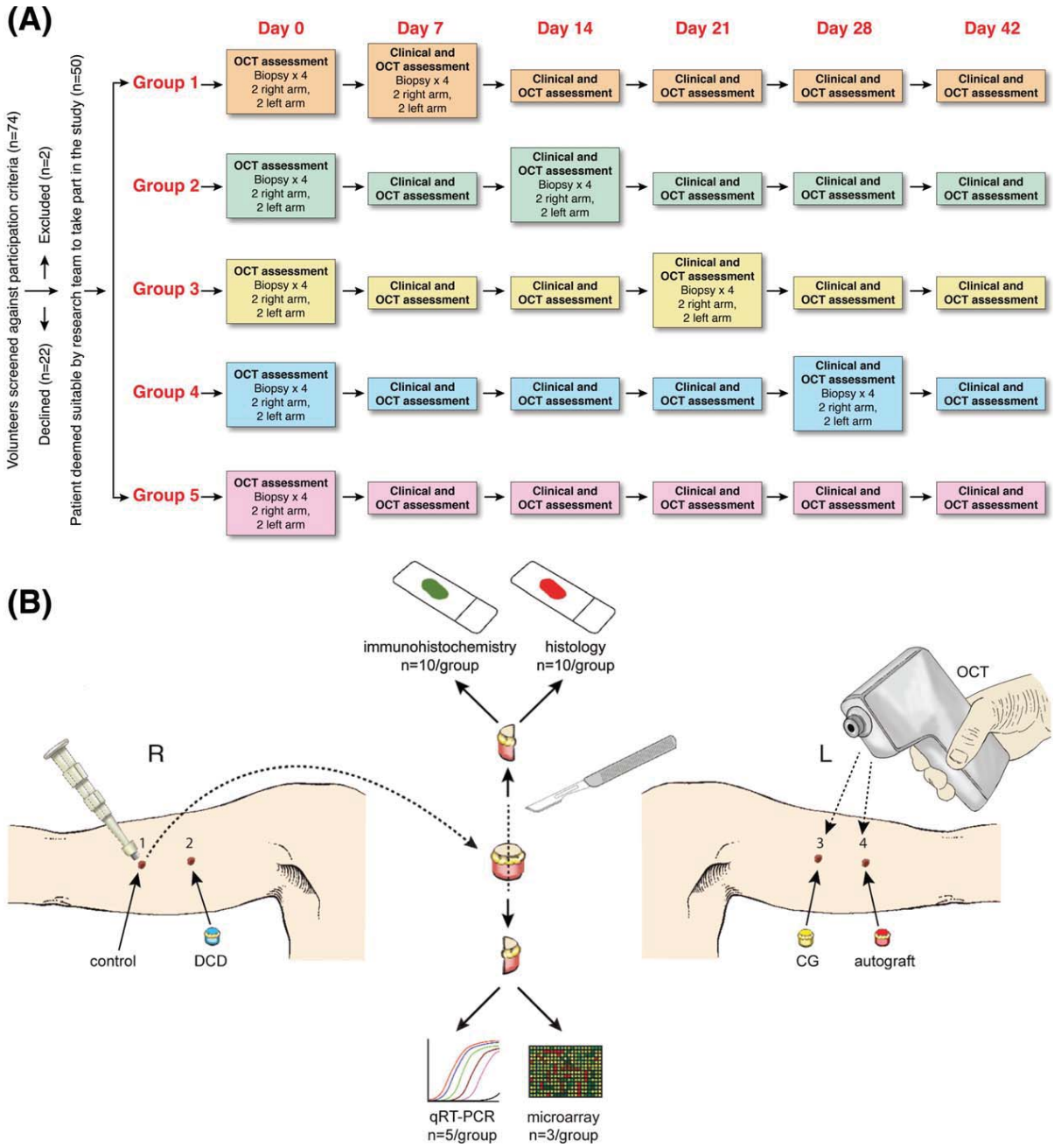

Figure 1. Prospective cohort study flowchart (A) and methodology (B). Seventy-four volunteers were screened, 2 were excluded, and 22 declined to take part. Fifty enrolled participants were electronically randomized to one of 5 groups, each containing 10 patients. On day 0, sites 1–4 were allocated and scanned using OCT before 5-mm punch biopsies were taken aseptically. Site 1 healed by secondary intention, site 2 was treated with CG, and site 3 treated with human DCD while excised tissue from site 4 was replaced into the defect (autograft). Subjects were followed-up for 42 days and OCT imaging repeated weekly. Six millimeter excision biopsies of healing tissue were harvested at time points based on study group allocation. All excised tissue was investigated using a range of laboratory techniques.

RNA extraction (n = 5 patients/group)

Biopsied tissues were homogenized in RLT buffer (Qiagen, GmbH, Helden, Germany) using steel beads and Qiagen TissueLyser II (Qiagen GmbH). RNA was extracted with RNeasy Fibrous Tissue Mini Kits (Qiagen GmbH) and Qiagen Qiacube (Qiagen GmbH). Eluted RNA

Table 1. Characteristics of volunteers within each study group

	Average Age (years)	Average BMI (m/kg^2)	Sex of Participants
Group 1	25.8	23.2	6 men 4 women
Group 2	33.7	25.6	4 men 6 women
Group 3	21.6	21.3	5 men 5 women
Group 4	24.7	22.4	3 men 7 women
Group 5	24.4	22.7	7 men 3 women

quantity and purity was assessed using NanoDrop ND-100 v3.0.1 spectrophotometer (NanoDrop Technologies, Wilmington, DE) and RNA integrity measured with Agilent 2100 Bioanalyser (Agilent Technologies, Wilmington, DE).

Microarray (n = 3 patients/group)

Microarrays were performed using Agilent Whole Human Genome (8X60K) Oligo Microarrays (Agilent Technologies) and the manufacturer's protocol (One-Color Microarray-Based Gene Expression Analysis – Version 6.5). Labeled complimentary-RNA from individual (non-pooled) donors was created using 50-ng RNA templates and Quick Amp Labeling Kits (One-Color; Agilent Technologies). Gene Expression Hybridization Kits (Agilent Technologies) were used; before, arrays were washed with Gene Expression Wash Buffer Kit solutions (Agilent Technologies). Arrays were scanned using Axon GenePix 4400A (Molecular Device Ltd, Wokingham, UK) and images extracted with GenePix Pro 7 (Molecular Device Ltd). Analyses were performed using BABELOMICS 4.3.0 gene expression and functional profiling analysis suite (http://babelomics.bioinfo.cipf.es).

qRT-pcr (n = 5 patients/group)

Expression of candidate and reference (ribosomal protein L32) genes was studied using real time polymerase chain reaction (qRT-PCR). One-microgram RNA and qScript cDNA Synthesis Kit (Quanta Biosciences, Gaithersburg, MD) were used to synthesize complementary-DNA. qRT-PCR reactions were carried out in triplicate using the Roche LightCycler 480 system (Roche Diagnostics GmBh).

STATISTICS

A sample size of 50 adequately powered statistical analysis designed to identify differences in primary and secondary outcomes between treatment groups. SPSS version 20 (IBM, Portsmouth, UK), and conventional two-sided 5% significance levels were used throughout. Initial analysis tested for an "arm effect" (left arm versus right arm) to rule out site-specific variation. For each variable, there was no significant difference between mean response on the left and right arms. On the basis that an arm effect was not statistically significant, further analysis was performed for each investigational modality looking for differences between treatment groups.

Dermal thickness

Analysis of variance (ANOVA) was used to test for differences between group mean dermal thickness values at each time point.

OCT and immunohistochemistry

Changes in values from d0 were analyzed separately for each treatment on different days using pairwise *t*-tests while differences between treatments at each time point were compared using ANOVA with Greenhouse-Geisser method. Time points with significant differences underwent additional pairwise comparisons, and Bonferroni adjustments were applied.

PCR

Nonparametric Friedman tests compared fold changes between treatments on d7, d14, d21, and d28 separately. If significant differences were found, paired Wilcoxon rank sum tests analyzed differences between modalities. Significant changes within treatment groups over time were assessed using one-sample Wilcoxon signed-rank tests.

Microarrays

GenePix .gpr files were normalized against one another using normexp background correction, implementing between array normalization by quantiles and excluding flagged spots from parameter fittings. Following normalization, data was additionally preprocessed with log2 transformation, merging redundant gene identifiers using the median value and imputing the row median where values were missing and requiring a gene identifier to have a value in at least 70% of arrays to be kept. Following data normalization and preprocessing, three analyses were performed. Limma was used to conduct pairwise comparisons of data from successive time points within each treatment group and data from each time point within a treatment group compared with d0 values. Furthermore, for each time point, all treatments were compared against each other using ANOVA analysis. In all comparisons, the Benjamini–Hochberg false discovery rate was controlled at 5%.

RESULTS

Study demographics

Seventy-four volunteers were screened for study enrolment. Seventy-two met suitability criteria but 22 declined. Twenty-four participants were male and 26 female. Mean age was 26 years and 92% of participants were white Caucasian (2% black Afro-Caribbean, 4% Asian [Chinese], and 2% Asian [Pakistani]). Characteristics including BMI, age, and sex were relatively homogenous between patient groups (Table 1). Complete data sets were collected with no loss to follow-up or adverse events.

Variations in cutaneous histology over time and between treatment groups

Control wounds developed a rim of serosanguinous infiltrate seven days after injury with subsequent progressive

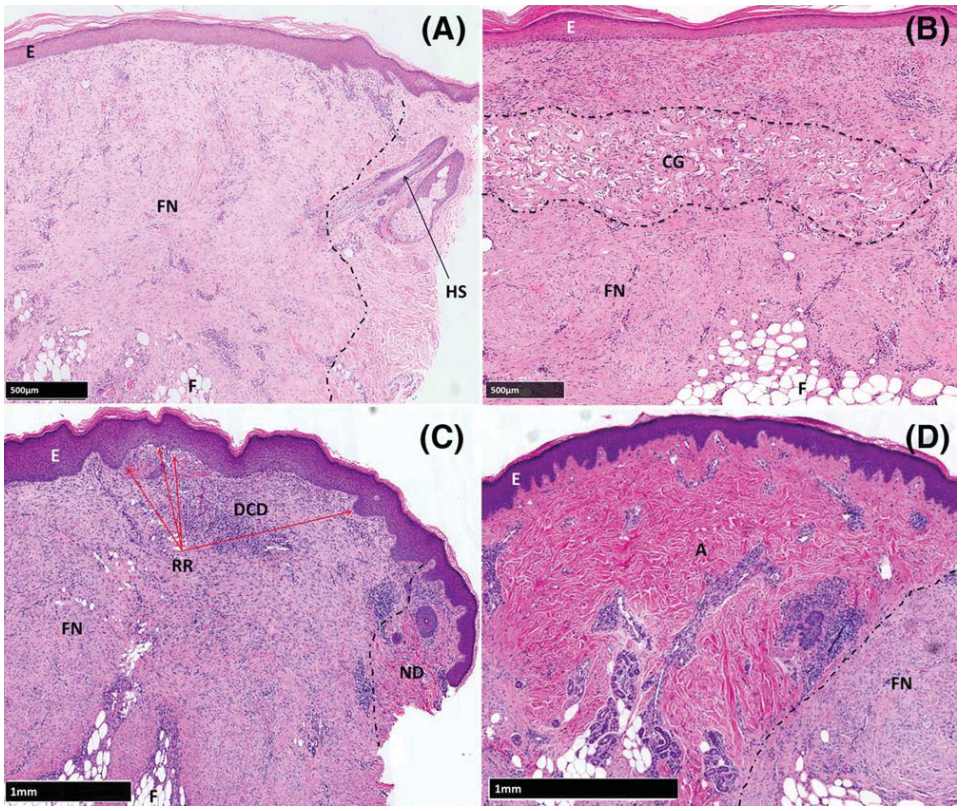

Figure 2. Comparative histology of samples from each treatment group, 28 days after injury. Control shows dense homogenous fibrosis with minor nodularity (A). CG displays a thick band of nodulofascicular fibrosis and characteristic biomaterial appearance (B). DCD illustrates dense cellular infiltrate, partial rete ridge reformation, and uniform fibrosis (C). Autograft displays retention of normal ECM architecture and minimal fibrosis in comparison to surrounding scar tissue (D). A – autograft, CG – collagen-GAG scaffold, DCD – decellularised dermis, E – epidermis, F – subcutaneous fat, FN – fibrotic neodermis, HS – hair shaft, ND – native dermis, and RR – rete ridges. Black dashes – define the wound margin in Figure 2A and the boundary between skin substitute and native tissue in Figure 2B.

deposition of ECM and expansion of granulation tissue with concurrent maturation resulting in homogenous bands of fibrosis with minor nodularity by d28 (Figure 2A). Spaces between CG fibers facilitated rapid early cellular influx by host cells, resulting in brisk diffuse formation of granulation tissue between fibrils. This tissue rapidly matured producing dense thick nodulofascicular fibrosis. CG was evident histologically throughout the study. Furthermore, there was dermal replacement superficial and deep to CG (Figure 2B). DCD showed slower but progressive colonization by native cells with formation of tongues of granulation tissue invading graft material at points defined by ECM fiber orientation. DCD samples formed uniform regions of fibrosis more slowly than CG and controls, punctuated by normally distributed blood vessels. DCD could not be distinguished from native dermis once infiltrated by host cells (Figure 2C). Autograft tissue appeared devitalized after injury with collapsed blood vessels, collagen denaturation, and epidermal atrophy. However, this reversed after vascular anastomoses formed at the graft/host interface re-establishing autograft circulation. Autografts subsequently developed minimal scarring associated with preservation of rete ridges, skin appendages, and differentiation between reticular and papillary dermis (Figure 2D). Control and CG samples lacked these features while half of DCD samples demonstrated partial reformation of rete ridges.

Quantification of dermal thickness

Autograft dermal thickness was significantly greater than controls at all time points ($p < 0.0001$), while DCD was significantly elevated compared with controls on d28 ($p = 0.003$; Figure 3).

Differences in structural protein expression

Collagen III was significantly reduced in controls compared with autografts on d7 and d14 ($p = 0.032$ and 0.011; Figure 4A). On d7, fibronectin was significantly higher in controls than DCD ($p = 0.022$) and on d21 compared with autografts ($p = 0.007$; Figure 4B). There were no significant differences in aSMA between treatments at any time point ($p = 0.316$, 0.221, 0.210, 0.063; Figure 4C). On d21, collagen I in controls was significantly higher than

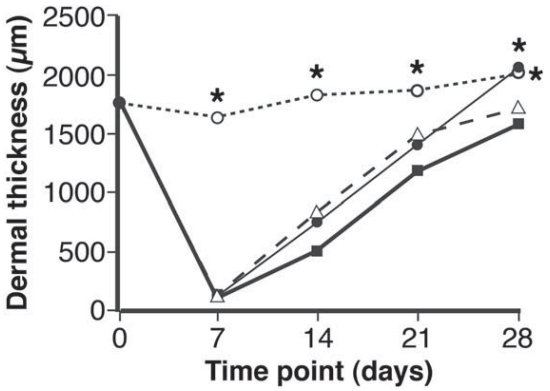

Figure 3. Change in dermal thickness over time. Control – solid line with squares, DCD – solid line with filled circles, CG – dashed line with triangles, and autograft – dashed line with open circles. *$p < 0.05$.

autografts ($p = 0.030$) while at d28, collagen I in CG was greater than autografts ($p = 0.047$; Figure 5A).

Changes in OCT derived MGV

MGV was significantly reduced from baseline in all treatment groups on d7–d21 (all $p < 0.001$). On d28, MGV was no different from baseline in controls, CG, and autografts ($p = 0.440$, 0.881, and 0.279) while it was significantly lower in DCD ($p < 0.001$). On d42, MGV was unchanged from baseline in autografts ($p = 0.685$) while it was significantly increased in controls, CG, and DCD ($p =$ 0.001, 0.001, and 0.022).

On d7–d21, autograft MGV was significantly greater than other modalities (all $p < 0.001$). MGV in DCD was elevated compared with controls ($p = 0.029$) at d7 while at d14 and d21, MGV in controls and CG was greater than DCD (all $p < 0.001$). On d28, values in DCD were significantly lower than other treatments ($p = 0.001$–0.002). However, on d42, autograft values were significantly lower than controls and CG while DCD ($p = 0.038$ and 0.015) was reduced compared with CG ($p = 0.017$; Figure 5B).

Visualization of cutaneous morphology using OCT

We previously showed that OCT can delineate morphology of normal skin and wounds throughout healing.[24] Fibrogenesis and scar formation are associated with progressive increases in tissue reflectivity (MGV) and a homogenous appearance correlating with ordered collagen bundles noted histologically (Figure 5C–F). Furthermore, skin substitute materials and cellular infiltration into biomaterials can be visualized (Figure 6A–F).

Differential genomic expression

Significantly altered expression of 58 genes associated with fibrosis was identified after injury (Supporting Information, Table S3). Twelve candidate genes were selected for qRT-PCR (interleukin-1b [IL1B], tumor necrosis factor [TNF], interleukin-10 [IL10], vascular endothelial growth factor-α [VEGFA], connective tissue growth factor [CTGF], matrix metalloproteinase 1 and 3 [MMP1,

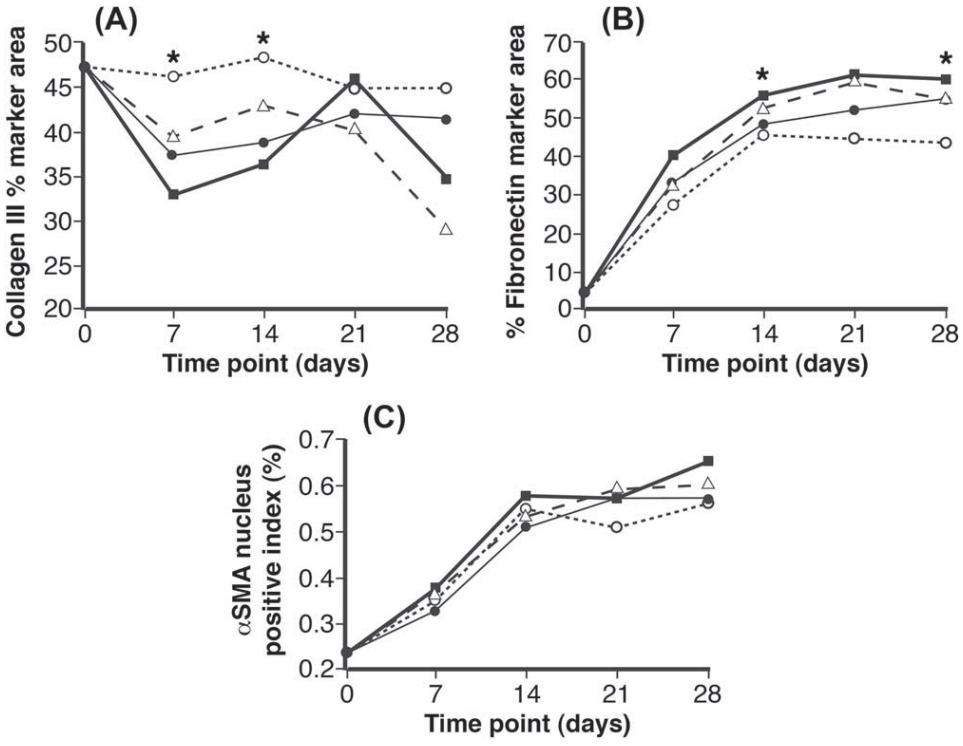

Figure 4. Changes in immunohistochemical marker expression over time. (A) Collagen III, (B) Fibronectin, and (C) αSMA. Control – solid line with squares, DCD – solid line with filled circles, CG – dashed line with triangles, and autograft – dashed line with open circles. *$p < 0.05$.

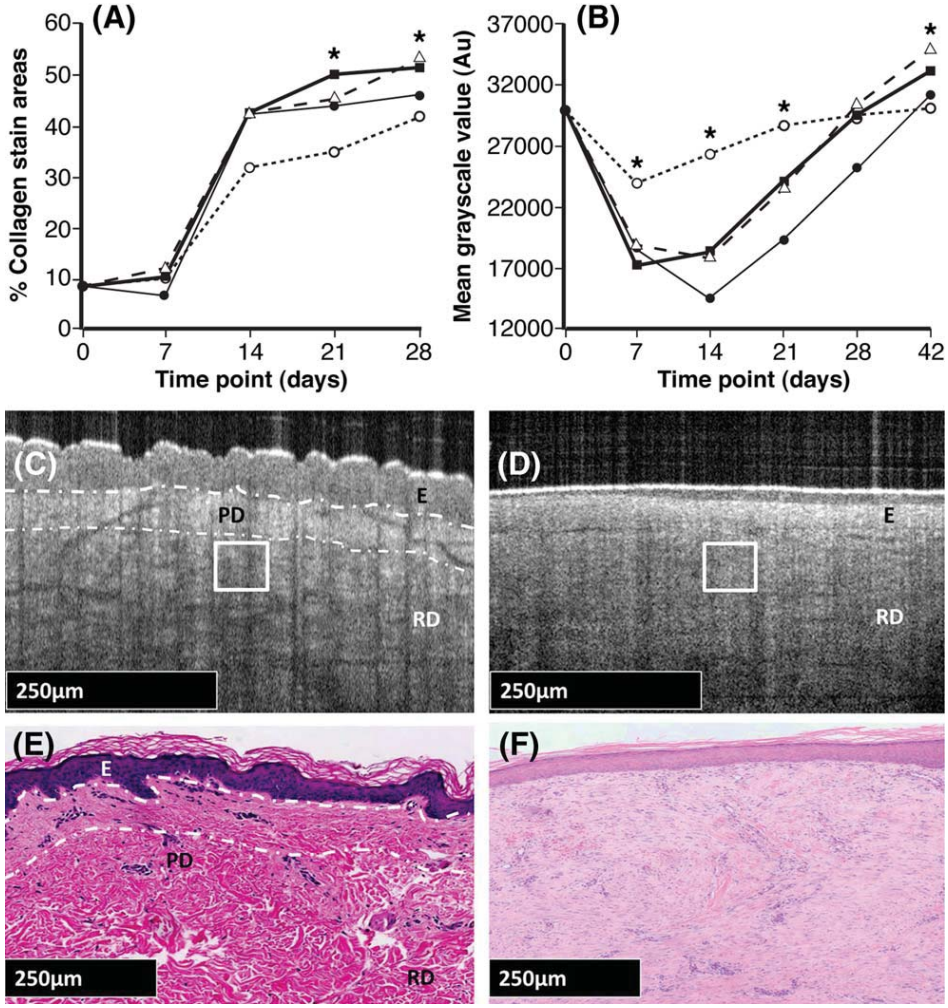

Figure 5. Invasive and non-invasive measures of fibrogenesis and scar tissue formation after injury. Collagen I immunohistochemical staining (A) and mean grayscale value (B) derived from OCT. OCT imaging and histological appearance of day 0 normal skin (C and E) and day 28 fibrotic wound tissue (D and F). Fibrotic tissue has a hyper-reflective appearance on OCT, with loss of distinction between dermal layers and numerous parallel collagen bundles. E – epidermis, PD – papillary dermis, RD – reticular dermis, and white square – representative of region where mean grayscale value measurement is taken. Control – solid line with squares, DCD – solid line with filled circles, CG – dashed line with triangles, and autograft – dashed line with open circles. $*p < 0.05$.

MMP3], oncostatin M [OSM], transforming growth factor-β1, 2, and 3 (TGFβ1, TGFβ2, TGFβ3), and lysyl oxidase [LOX]) to verify microarray data. These genes were selected based on a literature review for relevance to cutaneous fibrosis, previous experience with certain genes and availability of suitable primers.

Alterations in gene expression

On d21 ($p = 0.026$) and d28 ($p = 0.019$), IL1B expression was significantly greater in DCD than other treatments (Figure 7A). On d28 ($p = 0.033$), VEGFA expression was significantly greater in autografts than CG or DCD (Figure 7B). On d28 ($p = 0.019$), IL10 expression was significantly higher in DCD than other treatments (Figure 7C). On d14 ($p = 0.026$) and d21 ($p = 0.019$), OSM expression was significantly greater in DCD than other treatments (Figure 7D). On d21 ($p = 0.012$) and d28 ($p = 0.04$), MMP3 expression was significantly greater in DCD than controls and autografts while CG was elevated compared with controls (Figure 7E). On d14 ($p = 0.044$), d21 ($p = 0.019$), and d28 ($p = 0.007$), MMP1 expression was significantly greater in DCD than other treatments (Figure 7F). On d21 ($p = 0.041$), TGFβ2 expression was significantly lower in DCD than controls or autografts (Figure 7G). There were no significant differences in expression of LOX, CTGF, TGFβ1, TGFβ3, or TNF between treatment groups (Figure 7H–L).

DISCUSSION

Formation of fibrotic scar tissue is a normal response to dermal injury, but the influence of dSS on this process remains unclear.[4] Most data pertaining to dSS use in acute wounds is derived from animal studies hindered by small sample numbers, poor study design, and limited translation to human subjects.[22,23] In contrast, this unique study is the first to compare multiple treatment types in the same individuals over six weeks following cutaneous injury.

Fibrosis is an ill-defined term used to describe ECM deposition in a spectrum of conditions from normal wound healing to pathological scarring. Accurate quantitative

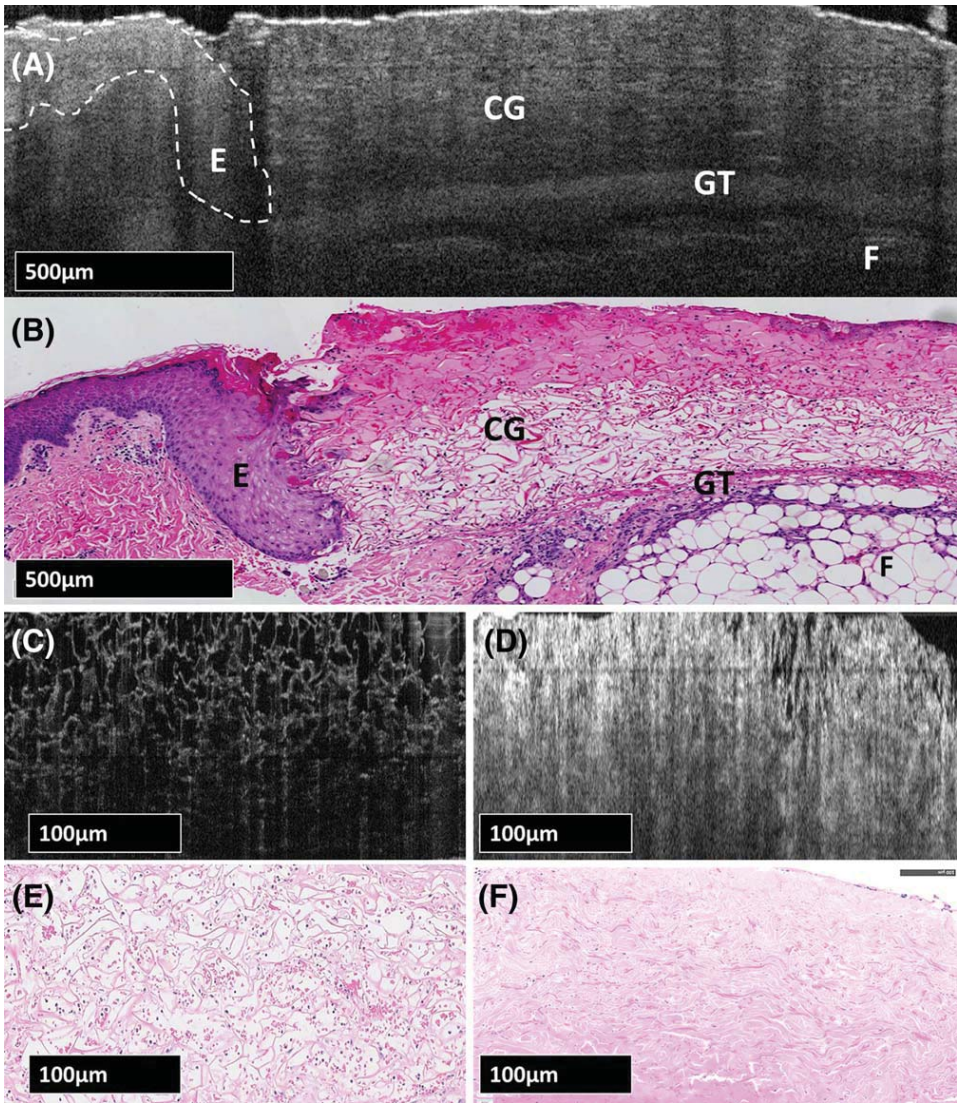

Figure 6. Time matched optical coherence image and histological sections. Day 7 CG sample illustrating good morphological congruity between investigative modalities (A and B). Comparative appearance of CG (C and E) and DCD (D and F) via OCT and histological sectioning demonstrating architectural differences between biomaterials. CG – collagen-GAG scaffold, E – epidermis, F – subcutaneous fat, and GT – granulation tissue. White dashed line – epithelial boundary.

fibrosis assessment tools are not available, and existing methods including the Vancouver scar scale and Manchester scar proforma have significant subjective elements.[4,25] In contrast, OCT is a noninvasive imaging technique analogous to ultrasound, that interferometrically detects infrared light and provides high resolution (1–7.5 μm) images of cutaneous ultrastructure.[25–27] MGV derived from OCT, alters during wound healing secondary to influxing cellular content as well as deposition and remodeling of ECM proteins.[24] It is not specific to any particular ECM component but provides an overview of all dermal constituents. This study confirms MGV can quantitatively assess the changing nature of ECM during dermal regeneration. Significant differences in MGV were identified between treatment groups that correlated with variations in tissue fibrosis identified by other means. Furthermore, OCT images corresponded to time-matched histology enabling concurrent assessment of wound morphology.[24] Larger evaluation studies are required, but OCT could reduce skin biopsy requirements while MGV may represent a novel quantitative measure of tissue fibrosis.[24]

OCT and laboratory studies demonstrated differential development of fibrotic tissue between treatments with best microscopic and macroscopic results in autograft samples (Figure 8). Autografts differ significantly from other biomaterials, with a full cellular complement, intact vasculature, and a reservoir of sequestered growth factors. Despite this, autograft behavior was histologically and genetically similar to other modalities seven days after injury. However, its characteristics changed significantly after formation of graft/host vascular anastomoses, thereby restoring circulatory integrity and improving graft viability. Resumption of blood flow within autografts is likely to have reduced angiogenic stimuli such as hypoxia. The influence of angiogenesis on fibrosis has been described previously.[28] Application of angiogenic

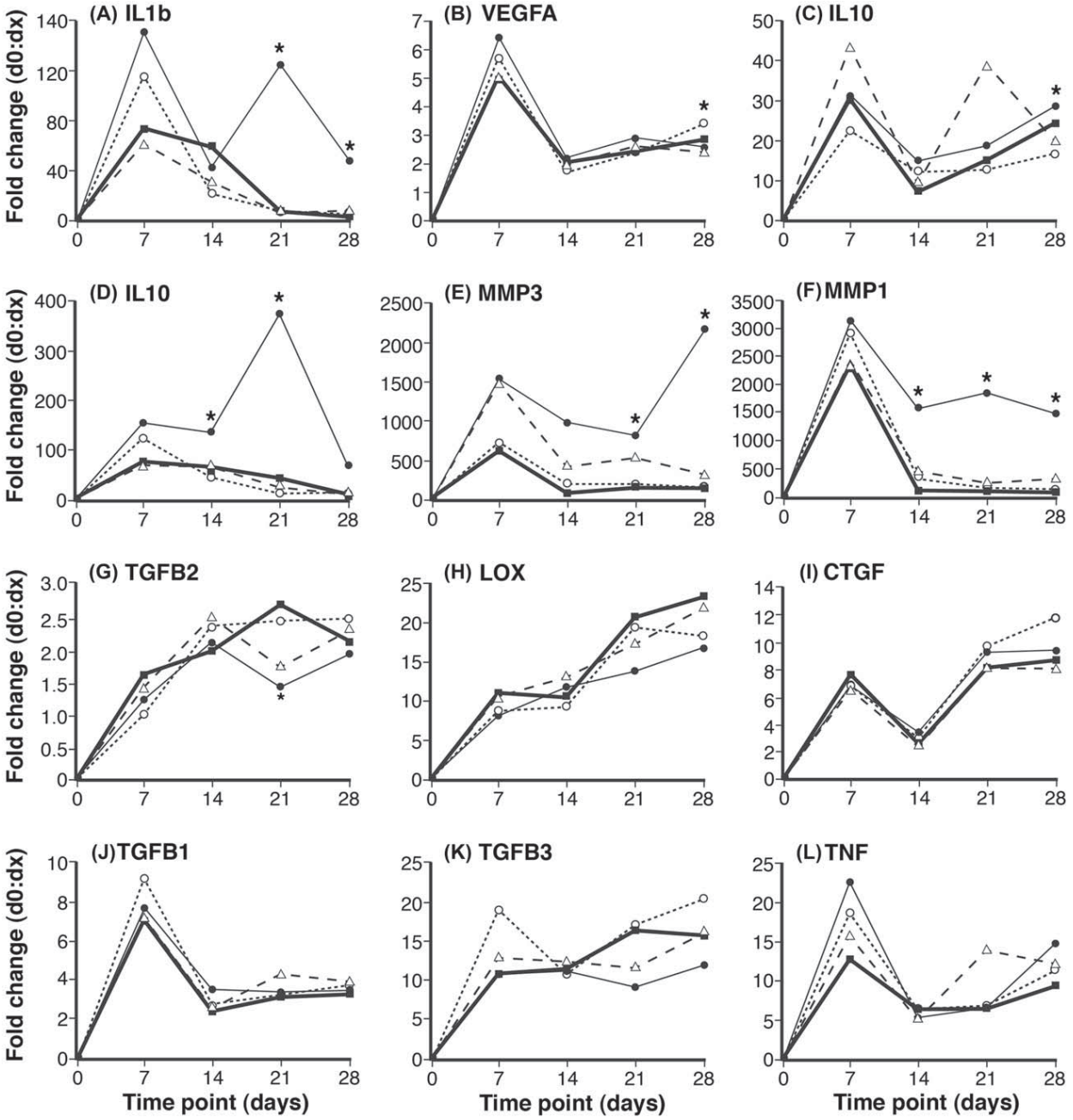

Figure 7. qRT-PCR of selected genes derived from whole genome microarray studies. (A) IL1B, (B) VEGFA, (C) IL10, (D) OSM, (E) MMP3, (F) MMP1, (G) TGFβ2, (H) LOX, (I) CTGF, (J) TGFβ1, (K) TGFβ3, and (L) TNF. Control – solid line with squares, DCD – solid line with filled circles, CG – dashed line with triangles, and autograft – dashed line with open circles. $^*p < 0.05$.

inhibitors to acute wounds such as endostatin reduced scar formation while proangiogenic molecules including IL-8 and TGF-β are found at lower concentrations during scarless fetal healing.[29–31] Consequently, reduced angiogenic drive in autografts after revascularization may contribute to subsequently limited scar formation. In contrast, other treatments require complete reconstitution of vascular networks resulting in prolongation of angiogenic signals with accordingly increased profibrotic side effects.

Autograft use is limited by volume of tissue that can be transplanted without a vascular pedicle and formation of another wound during tissue harvest. DCD represents an alternative therapeutic option, also associated with thicker neodermis and reduced fibrosis. DCD is a human tissue

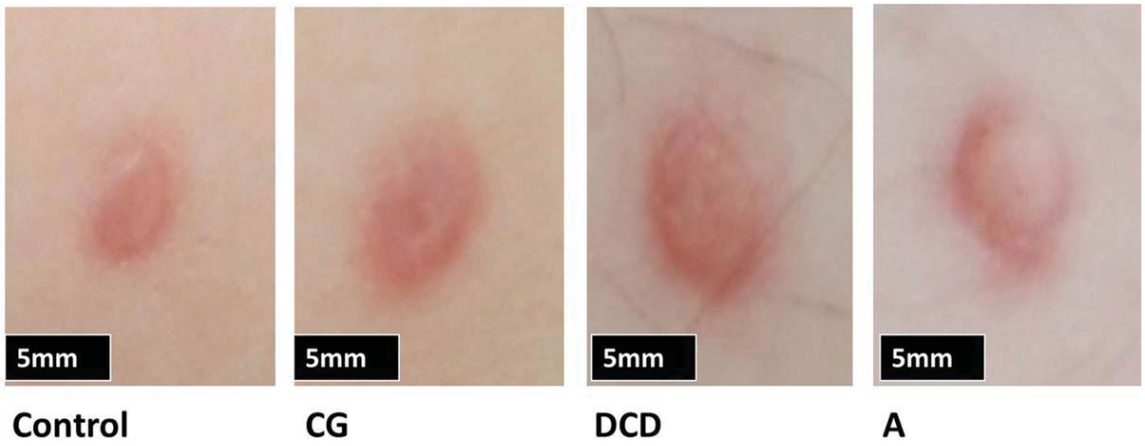

Figure 8. Differences in macroscopic appearances of healed punch biopsy wounds 42 days after injury.

allograft with inherently similar biomechanical and structural properties to autografts.[32] In contrast, CG does not have this architectural congruity as its constituent proteins are xenogenic in origin. ECM elasticity and porosity play key roles in regulating dynamic interactions between cells and matrix components as well as mediating binding or release of sequestered growth factors including TGF-β.[33] Consequently, ECM characteristics significantly influence infiltration and cellular positioning within matrices as well as proliferation, differentiation, and secretion profiles of resident cells.[34,35] In general, more rigid ECM like DCD promotes stable focal adhesions facilitating tissue formation while softer matrices such as CG encourage transient adhesions and increased cell motility.[36] In turn, cells exert contractile forces on ECM which modulate matrix components over time.[37] As a result, structural and biomechanical similarities between DCD and autografts may contribute to reduced fibrosis noted in these samples.

Progressive colonization of DCD by host cells resulted in unique bimodal expression of genes including OSM, IL10, IL1B, and MMP3. OSM is a potent mitogen for dermal fibroblasts and limits monocytic cell recruitment during inflammation via suppression of CCL5.[38] IL10 over expression is associated with reduced inflammatory mediators and promotion of regenerative healing while lower MMP3 levels are associated with impaired wound healing in mice and humans.[38–41] Late up-regulation of these genes was not observed in controls and this response may contribute to differences in observed outcomes.

Interestingly, expression of other key genes governing the fibrotic response such as TGFβ1 and TNF was similar between treatment groups within microarray and/or PCR studies. One explanation is that variations in fibrotic outcomes are secondary to novel unidentified bioactive substances. Other alternatives include differences in molecular profiles within the first week of treatment that were not assessed, being crucial in determining long-term fibrogenic behavior, particularly as this is the peak of the inflammatory period. Our sample size may have been under powered to detect differences in cytokine expression between treatment groups, and finally, mRNA expression is not always proportionally translated to active protein expression.[42] Dermal remodeling continues for many months after injury while the final time point in this study was 42 days. Consequently, we can only comment on initial outcomes recognizing that longer term follow-up, and further, biopsies would be beneficial to substantiate our findings. However, we have demonstrated for the first time that differences in fibrogenic behavior can be observed and measured from an early stage of wound healing. Further studies are required to validate these conclusions, investigate similar outcome measures at later time points and use such materials in larger, more diverse wounds.

In conclusion, treatment of acute cutaneous wounds with autografts or DCD resulted in reduced dermal fibrosis compared with equivalent injuries treated with CG and those healing by secondary intention. Differences in matrix composition, architecture, and cellular content between biomaterials may account for this variability. Although autografts are known to provide good cosmetic outcomes for injuries including burns, they have limited availability and are associated with significant morbidity. Consequently, our findings relating to DCD which is abundantly available off the shelf are particularly exciting, suggesting that DCD may stimulate a more regenerative rather than reparative therapeutic option in cutaneous wound management. Additionally, OCT is a novel, noninvasive method to evaluate tissue morphology and quantify wound fibrosis through MGV measurement. However, further randomized controlled studies are required to validate these findings and justify skin substitute and OCT use as therapeutic and diagnostic wound healing tools, respectively.

Acknowledgments

The authors gratefully acknowledge the support and help of Paul Cormack and Hamamatsu Photonics UK Ltd who facilitated digitalization of histological sections and Nanozoomer analysis software support. We would also like to thank Helen Carruthers, Katie Greaves, Ian Greaves and all the volunteers who took part.

Source of Funding: Partial funding for this study was provided by Tissue Regenix Ltd (York, UK) and Integra Matrix Wound Dressing was kindly provided by Integra LifeSciences (Plainsboro, NJ, USA).

Conflict of Interest: None of the authors have any commercial associations or financial disclosures and hence no conflict of interest.

Products used in the study: Integra Matrix Wound Dressing (Integra Lifesciences, Plainsboro, NJ)

National Health Service Blood and Transplant Decellularised Dermis (NHSBT, Watford, UK)

Reuse of data: Mean greyscale data for the control group was published previously in the British Journal of Dermatology (Optical coherence tomography: a reliable alternative to invasive histological assessment of acute wound healing in human skin. British Journal of Dermatology. 2014 Apr;170(4):840-50). It has been included in this submission as it is vital to enable comparison with skin substitute-assisted wound healing. It represents a small percentage of the total data presented in this paper.

REFERENCES

1. Eming SA, Krieg T, Davidson JM. Inflammation in wound repair: molecular and cellular mechanisms. *J Invest Dermatol* 2007; 127: 514–25.
2. Nelson CM, Bissell MJ. Of extracellular matrix, scaffolds, and signaling: tissue architecture regulates development, homeostasis, and cancer. *Annu Rev Cell Dev Biol* 2006; 22: 287.
3. Diegelmann RF, Evans MC. Wound healing: an overview of acute, fibrotic and delayed healing. *Front Biosci* 2004; 9: 283–9.
4. Bayat A, McGrouther D, Ferguson M. Skin scarring. *BMJ* 2003; 326: 88–92.
5. Metcalfe AD, Ferguson MW. Tissue engineering of replacement skin: the crossroads of biomaterials, wound healing, embryonic development, stem cells and regeneration. *J R Soc Interface* 2007; 4: 413–37.
6. Larson BJ, Longaker MT, Lorenz HP. Scarless fetal wound healing: a basic science review. *Plast Reconstr Surg* 2010; 126: 1172.
7. Mori R, Power KT, Wang CM, Martin P, Becker DL. Acute downregulation of connexin43 at wound sites leads to a reduced inflammatory response, enhanced keratinocyte proliferation and wound fibroblast migration. *J Cell Sci* 2006; 119: 5193–203.
8. Martin P, D'Souza D, Martin J, Grose R, Cooper L, Maki R, et al. Wound healing in the PU. 1 null mouse—tissue repair is not dependent on inflammatory cells. *Curr Biol* 2003; 13: 1122–8.
9. Manuel JA, Gawronska-Kozak B. Matrix metalloproteinase 9 (MMP-9) is upregulated during scarless wound healing in athymic nude mice. *Matrix Biol* 2006; 25: 505–14.
10. Gawronska-Kozak B, Bogacki M, Rim JS, Monroe WT, Manuel JA. Scarless skin repair in immunodeficient mice. *Wound Repair Regen* 2006; 14: 265–76.
11. Rhett JM, Ghatnekar GS, Palatinus JA, O'Quinn M, Yost MJ, Gourdie RG. Novel therapies for scar reduction and regenerative healing of skin wounds. *Trends Biotechnol* 2008; 26: 173–80.
12. Stoff A, Rivera AA, Mathis JM, Moore ST, Banerjee N, Everts M, et al. Effect of adenoviral mediated overexpression of fibromodulin on human dermal fibroblasts and scar formation in full-thickness incisional wounds. *J Mol Med* 2007; 85: 481–96.
13. Rodgers KE, Roda N, Felix JC, Espinoza T, Maldonado S, DiZerega G. Histological evaluation of the effects of angiotensin peptides on wound repair in diabetic mice. *Exp Dermatol* 2003; 12: 784–90.
14. Witte MB, Thornton FJ, Kiyama T, Efron DT, Schulz GS, Moldawer LL, et al. Metalloproteinase inhibitors and wound healing: a novel enhancer of wound strength. *Surgery* 1998; 124: 464–70.
15. Iocono JA, Ehrlich HP, Keefer KA, Krummel TM. Hyaluronan induces scarless repair in mouse limb organ culture. *J Pediatr Surg* 1998; 33: 564–7.
16. MacNeil S. Progress and opportunities for tissue-engineered skin. *Nature* 2007; 445: 874–80.
17. Mostow EN, Haraway GD, Dalsing M, Hodde JP, King D. Effectiveness of an extracellular matrix graft (OASIS Wound Matrix) in the treatment of chronic leg ulcers: a randomized clinical trial. *J Vasc Surg* 2005; 41: 837–43.
18. Winters CL, Brigido SA, Liden BA, Simmons M, Hartman JF, Wright ML. A multicenter study involving the use of a human acellular dermal regenerative tissue matrix for the treatment of diabetic lower extremity wounds. *Adv Skin Wound Care* 2008; 21: 375.
19. Greaves NS, Iqbal SA, Baguneid M, Bayat A. The role of skin substitutes in the management of chronic cutaneous wounds. *Wound Repair Regen* 2013; 21: 194–210.
20. Rehfeldt F, Engler AJ, Eckhardt A, Ahmed F, Discher DE. Cell responses to the mechanochemical microenvironment—implications for regenerative medicine and drug delivery. *Adv Drug Deliv Rev* 2007; 59: 1329–39.
21. Engler AJ, Sen S, Sweeney HL, Discher DE. Matrix elasticity directs stem cell lineage specification. *Cell* 2006; 126: 677–89.
22. Moiemen N, Yarrow J, Hodgson E, Constantinides J, Chipp E, Oakley H, et al. Long-term clinical and histological analysis of Integra dermal regeneration template. *Plast Reconstr Surg* 2011; 127: 1149–54.
23. Truong AT, Kowal-Vern A, Latenser BA, Wiley DE, Walter RJ. Comparison of dermal substitutes in wound healing utilizing a nude mouse model. *J Burns Wounds* 2005; 4: e4.
24. Greaves N, Benatar B, Whiteside S, Alonso-Rasgado T, Baguneid M, Bayat A. Optical coherence tomography: a reliable alternative to invasive histological assessment of acute wound healing in human skin? *Br J Dermatol* 2013; 170: 840–50.
25. Powers PS, Sarkar S, Goldgof DB, Cruse CW, Tsap LV. Scar assessment: current problems and future solutions. *J Burn Care Res* 1999; 20: 54–60.
26. Gambichler T, Jaedicke V, Terras S. Optical coherence tomography in dermatology: technical and clinical aspects. *Arch Dermatol Res* 2011; 303: 457–73.
27. Welzel J, Reinhardt C, Lankenau E, Winter C, Wolff H. Changes in function and morphology of normal human skin: evaluation using optical coherence tomography. *Br J Dermatol* 2004; 150: 220–5.
28. Greaves NS, Ashcroft KJ, Baguneid M, Bayat A. Current understanding of molecular and cellular mechanisms in fibroplasia and angiogenesis during acute wound healing. *J Dermatol Sci* 2013; 72: 206–17.
29. Bloch W, Huggel K, Sasaki T, Grose R, Bugnon P, Addicks K, et al. The angiogenesis inhibitor endostatin impairs blood vessel maturation during wound healing. *FASEB J* 2000; 14: 2373–6.

30. Liu W, Wang D, Cao Y. TGF-beta: a fibrotic factor in wound scarring and a potential target for anti-scarring gene therapy. *Curr Gene Ther* 2004; 4: 123–36.
31. Liechty KW, Crombleholme TM, Cass DL, Martin B, Adzick NS. Diminished interleukin-8 (IL-8) production in the fetal wound healing response. *J Surg Res* 1998; 77: 80–4.
32. Hogg P, Rooney P, Ingham E, Kearney JN. Development of a decellularised dermis. *Cell Tissue Bank* 2012; 14: 465–74.
33. Wipff P-J, Rifkin DB, Meister J-J, Hinz B. Myofibroblast contraction activates latent TGF-β1 from the extracellular matrix. *J Cell Biol* 2007; 179: 1311–23.
34. Ma L, Gao C, Mao Z, Zhou J, Shen J, Hu X, et al. Collagen/chitosan porous scaffolds with improved biostability for skin tissue engineering. *Biomaterials* 2003; 24: 4833–41.
35. Beningo KA, Dembo M, Wang Y-L. Responses of fibroblasts to anchorage of dorsal extracellular matrix receptors. *Proc Natl Acad Sci USA* 2004; 101: 18024–9.
36. Nicolas A, Safran SA. Limitation of cell adhesion by the elasticity of the extracellular matrix. *Biophys J* 2006; 91: 61–73.
37. Kreis TE, Birchmeier W. Stress fiber sarcomeres of fibroblasts are contractile. *Cell* 1980; 22: 555–61.
38. Ihn H, Tamaki K. Oncostatin M stimulates the growth of dermal fibroblasts via a mitogen-activated protein kinase-dependent pathway. *J Immunol* 2000; 165: 2149–55.
39. Dumas A, Lagarde S, Laflamme C, Pouliot M. Oncostatin M decreases interleukin-1 β secretion by human synovial fibroblasts and attenuates an acute inflammatory reaction in vivo. *J Cell Mol Med* 2012; 16: 1274–85.
40. Bullard KM, Lund L, Mudgett JS, Mellin TN, Hunt TK, Murphy B, et al. Impaired wound contraction in stromelysin-1–deficient mice. *Ann Surg* 1999; 230: 260.
41. Utz ER, Elster EA, Tadaki DK, Gage F, Perdue PW, Forsberg JA, et al. Metalloproteinase expression is associated with traumatic wound failure. *J Surg Res* 2010; 159: 633–9.
42. Lord P, Wilmoth L, Mizel S, McCall C. Expression of interleukin-1 alpha and beta genes by human blood polymorphonuclear leukocytes. *J Clin Invest* 1991; 87: 1312.
43. Welzel J. Optical coherence tomography in dermatology: a review. *Skin Res Technol* 2001; 7: 1–9.

Supporting Information

Additional Supporting Information may be found in the online version of this article.

Table S1. List of inclusion and exclusion criteria for the study.

Table S2. List of antibodies and staining regimes used in the immunohistochemical studies.

Table S2. List of genes highlighted in microarray studies known to be associated with fibrogenesis.